CrystEngComm

Accepted Manuscript

ROYAL SOCIETY OF CHEMISTRY

www.rsc.org/crystengcomm

CrystEngComm

RSCPublishing

ARTICLE

Tuning the Porosity through Interpenetration on Azobenzene-4,4'-Dicarboxylate based Metal-Organic Frameworks

Cite this: DOI: 10.1039/xoxxoooooox

Received ooth January 201X,
Accepted ooth January 201X

DOI: 10.1039/xoxxoooooox

www.rsc.org/

Belén Fernández,[a] José Manuel Seco,[b] Javier Cepeda,[*,b,c] Antonio J. Calahorro,[a] and Antonio Rodríguez-Diéguez[*,a]

A series of zinc(II) or cadmium(II) based compounds with elongated dicarboxylate and bipyridine ligands, namely, {dma[Cd(μ-azdc)(μ-ac)]·xDMF}$_n$ (**1**), {[Cd$_2$(μ$_4$-azdc)(μ-azdc)(DMSO)$_4$]·DMSO}$_n$ (**2**), [Cd$_3$(μ$_4$-azdc)$_3$(DMF)$_2$]$_n$ (**3**), {[Zn$_2$(μ$_3$-azdc)$_2$(μ-pbptz)]·xDMF}$_n$ (**4**), and {[Zn$_3$(μ$_4$-azdc)$_3$(μ-pbptz)$_2$]·xDMF·yH$_2$O}$_n$ (**5**) (where dma = dimethylammonium, azdc = azobenzene-4,4'-dicarboxylate, ac = acetate, DMF = dimethylformamide, DMSO = dimethylsulfoxide, pbptz = 3,6-bis(4-pyridyl)-1,2,4,5,-tetrazine) have been synthesized under solvothermal conditions and structurally characterized by single crystal X-ray diffraction. Crystal structures range from 2D to 3D systems according to the presence of the pbptz coligand, which aids the layers established by the azdc ligands to increase their dimensionality. The structural diversity found in each system is the result of three factors that govern the assembling process by modulating the coordination mode of azdc ligands: the employed solvent, counterion and metal:ligand stoichiometry. A common structural feature for these compounds is the highly open architectures achieved owing to the length of the employed ligands, which favours the resulting frameworks to be interpenetrated with different degrees depending on the network topology. A careful computational analysis of the void systems of compounds permits establishing a relationship of this phenomenon with the pore size. Photoluminescence properties of all compounds have been also investigated.

1. Introduction

Metal–organic frameworks (MOFs) are porous inorganic–organic hybrid materials, often considered as a subclass of coordination polymers, which are constructed from metal ions or clusters and organic ligands linked via coordination bonds to form polymeric systems.[1] These materials have received considerable attention in chemical and materials sciences not only due to their intriguing structural topologies but also because of their potential as functional materials in structure-dependent applications, such as gas storage and separation,[2] sensing,[3] catalysis,[4] and drug delivery,[5] as well as various proof-of-concept demonstrations.[6] Being generally constructed by inorganic vertices (metal ions or clusters) and organic linkers, one of their most attractive features, in addition to their crystalline nature, arises from the versatile chemistry and tailorable structures that provide a significant level of tuneable and permanent porosity provided a judicious selection of the starting components has been initially done. In fact, a longer organic linker usually provides larger porosity, so MOFs exhibiting exceptional porosity (up to 90%) and a high surface area (up to *ca.* 7000 m^2/g) are already known.[7] However, long organic linkers often lead to interpenetrating frameworks,[8] more accurately described as interwoven, in which two separate frameworks self-assemble within each other. In MOF chemistry, control of the interpenetration is of high importance because the degree of interpenetration significantly affects the gas sorption properties of the material.[9] There have been a few reports of methods to control the interpenetration of MOFs, including the addition of a template during the synthesis,[10] rational design of ligands,[11] and adjustment of the reaction conditions, such as the concentration of building blocks and temperature,[12] yet this issue is only solved for some particular systems. In contrast to the predictions made by theoretical calculations performed up to date,[13] experimental adsorption data have shown that interpenetrated frameworks could perform as better adsorbents in spite of the reduction of porosity of frameworks. In this regard, H_2 adsorption experiments on catenated PCN-6 and non-catenated PCN-6' stand as good example, since the interaction between the adsorbate molecules and the organic linkers becomes stronger in catenated PCN-6 than in PCN-6' once the open-metal sites of the structure have been occupied.[14]

Taking these considerations into account, we selected azobenzene-4,4'-dicarboxylate (azdc) as linker given its high potential to build open architectures due to the length of the spacer and the opposed disposition of the carboxylate groups.[15] Carboxylates are attractive metal binding units in coordination networks due to the negative charge that significantly enhances their ability to bind strongly to metal centres. This feature undoubtedly contributes to the robust nature of the resulting coordination networks. Moreover, diversified coordination modes (monodentate, chelating, and/or bridging) of carboxylates allow accessing to a wide variety of structures. In fact, their linkage to metal atoms with a high coordination plasticity, such as cadmium(II) and zinc(II), favours the structural diversity to take place just by introducing subtle changes in the synthetic conditions or an additional ligand that could play the opposing role. In this sense, N-donor ligands are good candidates since they establish fixed coordination patterns, among which acting as pillaring linker is the preferred one. As a result, five new compounds with intriguing frameworks have been synthesised and characterised. Most of them possess open architectures despite the occurrence of interpenetration. Photoluminescence measurements have been accomplished as well on the solid samples in order to verify the ligand-to-metal charge transfer mechanism associated with d^{10} transition metal based MOFs.[16]

2. Experimental section

All reagents and solvents were commercially available and used directly without any further purification.

2.1. Synthesis of compounds.

2.1.1.Synthesis of $\{dma[Cd(\mu\text{-azdc})(\mu\text{-ac})]\cdot xDMF\}_n$ (**1**)

0.014 g of azobenzene-4,4'-dicarboxylic acid (H_2azdc) (0.05 mmol) were added to 2mL of DMF. The resulting solution was sonicated for 10 minutes, and then 0.013g $Cd(AcO)_2\cdot 2H_2O$ (0.05 mmol) dissolved in 2 mL DMF were added. The reaction mixture was heated in a closed vial at 95 °C in oven for 48 h. Orange crystals were obtained. Yield: 42% based on Cd.

2.1.2. Synthesis of $\{[Cd_2(\mu_4\text{-azdc})(\mu\text{-azdc})(DMSO)_4]\cdot DMSO\}_n$ (**2**)

Compound **2** was prepared following the same procedure of compound **1** but using DMSO as solvent. Yield: 65% based on Cd.

2.1.3. Synthesis of $[Cd_3(\mu_4\text{-azdc})_3(DMF)_2]_n$ (**3**)

Compound **3** was prepared in a similar way to compound **1**, but cadmium nitrate tetrahydrate (0.015 g, 0.05 mmol) was used instead of cadmium acetate dihydrate. Orange crystals were obtained. Yield: 51% based on Cd.

2.1.4. Synthesis of $\{[Zn_2(\mu_3\text{-azdc})_2(\mu\text{-pbptz})]\cdot xDMF\}_n$ (**4**)

0.013 g of $Zn(NO_3)_2\cdot 4H_2O$ (0.05 mmol) were added to 2 ml of an orange solution of DMF containing 0.007 g of H_2azdc (0.025 mmol). The resulting solution was sonicated for 10 minutes, and then 0.006 g of 3,6-bis(4-pyridyl)-1,2,4,5,-tetrazine (pbptz) (0.025 mmol) dissolved in 2 mL of DMF were added. The reaction mixture was heated in a closed vial at 95°C in oven for 48h. Light pink crystals of compound **4** were obtained. Yield: 42% based on Zn.

2.1.5. Synthesis of $\{[Zn_3(\mu_4\text{-azdc})_3(\mu\text{-pbptz})_2]\cdot 4DMF\cdot 6H_2O\}_n$ (**5**)

Light orange crystals of compound **5** were obtained following the same procedure detailed for compound **4** but employing 0.05 mmol of each reagent in a 1:1:1 stoichiometry of Zn:azdc:pbptz. Yield: 43% based on Zn.

2.2. Single-crystal X-ray diffraction.

X-ray data collection of suitable single crystals were done at 100(2) K on a Bruker AXS APEX CCD area detector equipped with graphite monochromated Mo-Kα radiation (λ = 0.71073 Å) by applying the ω-scan method. The data reduction was performed with the APEX2[17] software and corrected for absorption using SADABS.[18] Crystal structures were solved by direct methods using the SIR97 program[19] and refined by full-matrix least-squares on F^2 including all reflections using anisotropic displacement parameters by means of the WINGX crystallographic package.[20] All hydrogen atoms were located in difference Fourier maps and included as fixed contributions riding on attached atoms with isotropic thermal displacement parameters 1.2 times or 1.5 times those of their parent atoms for the organic ligands and the water molecules, respectively. During the refinement of compounds **1**, **4**, and **5** the electron density at the voids was subtracted from the reflection data by the SQUEEZE procedure as implemented in PLATON program[21] due to the presence of disordered solvent molecules. Details of the structure determination and refinement of all compounds are summarized in Table 1. CCDC 1415511-1415515 contain the supplementary crystallographic data for this paper. These data can be obtained free of charge via http://www.ccdc.cam.ac.uk/conts/retrieving.html (or from the Cambridge Crystallographic Data Centre, 12, Union Road, Cambridge CB2 1EZ, UK; fax: +44 1223 336033). Deposited data may be accessed by the journal and checked as part of the refereeing process. If data are revised prior to publication, a replacement file should be sent to CCDC.

Table 1. Crystallographic data and structure refinement details of all compounds.

	1	2	3	4	5
Chem. formula	$C_{18}H_{19}CdN_3O_6$	$C_{38}H_{46}CdN_4O_{13}S_5$	$C_{48}H_{38}Cd_3N_8O_{14}$	$C_{20}H_{12}N_5O_4Zn$	$C_{60}H_{36}N_{14.5}O_{12}Zn$
Formula weight	480.73	1151.94	1288.09	451.72	1348.14
Crystal system	Orthorhombic	Monoclinic	Triclinic	Monoclinic	Triclinic
Superspace group	*C*mca	*C*2/c	*P*–1	$P2_1$/c	*P*–1
a (Å)	30.09(3)	31.831(6)	10.7515(7)	6.981(1)	16.945(5)
b (Å)	17.23(2)	7.884(2)	10.7424(7)	26.778(4)	16.958(5)
c (Å)	8.658(7)	19.449(4)	11.0098(8)	13.660(2)	17.880(5)
α(°)	90	90	95.683(2)	90	83.348(7)
β(°)	90	107.912(6)	96.940(2)	98.150(5)	73.542(7)
γ(°)	90	90	96.596(2)	90	65.791(7)
V (Å^3)	4488(7)	4644(3)	1245.7(2)	2527.8(6)	4494(5)
Z	8	4	1	4	2
GOF [a]	1.097	1.029	1.068	1.006	0.880
R_{int}	0.0639	0.1320	0.0259	0.0507	0.1364
R_1 [b] / wR^2 [c] [I>2σ(I)]	0.1524 / 0.3267	0.0695 / 0.1281	0.0176 / 0.0425	0.0612 / 0.1436	0.0916 / 0.2381
R_1 [b] / wR^2 [c] (all data)	0.1623 / 0.3321	0.1353 / 0.1455	0.0193 / 0.0433	0.1002 / 0.1560	0.1470 / 0.2653

[a] $S = [\sum w(F_0^2 - F_c^2)^2 / (N_{obs} - N_{param})]^{1/2}$ [b] $R_1 = \sum||F_0|-|F_c|| / \sum|F_0|$ [c] $wR^2 = [\sum w(F_0^2 - F_c^2)^2 / \sum wF_0^2]^{1/2}$; $w = 1/[\sigma^2(F_0^2) + (aP)^2 + bP]$ where $P = (\max(F_0^2,0) + 2Fc^2)/3$ with a = 0.0791 (**1**), 0.0547 (**2**), 0.0158 (**3**), 0.1154 (**4**), 0.1548 (**5**), and b = 514.1306 (**1**), 8.7623 (**2**), 1.3588 (**3**).

2.3. Photoluminescence measurements.

A Varian Cary-Eclipse Fluorescence Spectrofluorimeter was used to obtain the fluorescence spectra. The spectrofluorimeter was equipped with a xenon discharge lamp (peak power equivalent to 75 kW), Czerny-Turner monochromators, R-928 photomultiplier tube which is red sensitive (even 900 nm) with manual or automatic voltage controlled using the Cary Eclipse software for Windows

95/98/NT system. The photomultiplier detector voltage was 700 V and the instrument excitation and emission slits were set at 5 and 5 nm, respectively.

3. Results and Discussion

3.1. Comments on the Cd/azdc and Zn/azdc/pbptz systems.

X-ray diffraction analyses revealed the occurrence of five different product phases that are classified in the Cd/azdc and Zn/azdc/pbptz systems. The structural diversity found in these systems can be explained according to different factors that are imposed by the synthetic conditions that affect the coordination mode of the azdc ligands (Scheme 1). To start with, the three compounds obtained in the Cd/azdc system share the structural feature of being built up from 2D networks, although their packing gives rise to remarkably different overall frameworks with variable pore sizes left by different degrees of interpenetration. In particular, there are two factors that govern the assembling process: employed solvents and counterions of the metal salt. On the one hand, it is well known that DMF under solvothermal conditions tends to undergo hydrolysis reaction, obtaining formate anions and dimethylammonium cations as byproducts.[22] Therefore, when this solvent is used to dissolve $Cd(AcO)_2$ and H_2azdc, dma cations seem to template an open network formed by the azdc ligands (which acquire the coordination mode *b*) in which acetate anions are forced to act as bridging ligands in order to balance a neutral charge of compound **1**. Nevertheless, using a solvent that remains stable and neutral upon heating, such as DMSO, prevents the incorporation of acetate anions in the structure, in such a way that in the resulting open 2D network of **2** azdc ligands are obliged to increase their denticity (coordination mode *c*). On the other hand, the presence of nitrate anions in the reaction media (with a lower coordination capacity) do not take part in the crystal structure, thus preventing the templating effect of the dma cations, despite their generation during solvothermal reaction. As a result, the compact network achieved leaves no voids in the overall packing of compound **3**.

The addition of pbptz co-ligand to the reaction media, which has a preferred coordination mode and a marked trend to act as a pillar, gives, as expected, 3D primitive cubic type (α-Po) structures in the Zn/azdc/pbptz system.[23] In this MOFs, 2D layers are assembled from paddle-wheel cluster units $[M_2(O_2CR)_4]$ (M= Cu^{2+}, Zn^{2+}, and Co^{2+}) and dicarboxylate linkers. The 2D layers are linked with pillars to form 3D MOFs in which the pore size and environment can be simply tuned by selecting the different combinations of dicarboxylates and pillar linkers. Following this criterion, it has been given access to the porous framework of **5**, which contains triply interpenetrated 3D networks given the length of the connectors and their disposition. This architecture requires a Zn:azdc:pbptz stoichiometry of 1:1:1. However, when the proportion of the metal is doubled, the high flexibility of the azdc ligands together with the plasticity of the Zn(II) atoms allows obtaining a structure that maintains the topology whereas the interpenetration is increased up to 4-fold.

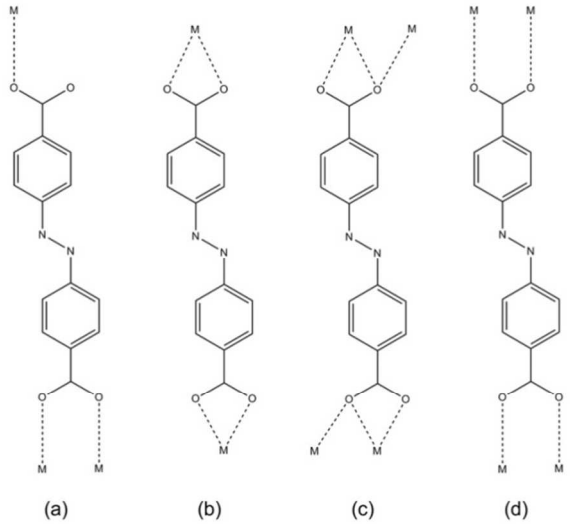

Scheme 1. Coordination modes of the azdc ligand in compounds **1**–**5**.

3.2. Description of the structures.

Compound **1** consists of open and planar 2D layers based on centrosymmetric dinuclear building units. Within the units, two symmetrically equivalent Cd1 atoms are doubly bridged through the oxygen atoms of two μ-acetate anions (Cd1···Cd1 of 3.56 Å). Given the coordination mode of these anions, in which only one atom is anchored to the metals, the remaining oxygen and carbon atoms can freely occupy both positions, thus causing the anions to be disordered. The severely distorted trigonal prismatic environment of the metal atom (S_{TPR} = 3.31) is completed by four oxygen atoms of two chelating carboxylate groups of two μ-azdc ligands. Cd–O coordination bonds are similar to those found for previously reported compounds with similar carboxylic ligands (Table 2).[24] *Trans*-$azdc^{2-}$ ligands are essentially planar except for the hydrazine function that lies out of the parallel 4-benzenecarboxylate moieties and imposes a separation of 0.263 Å between them (Figure 1). Four azdc ligands emerge from the edges of the dinuclear core, which can be referred to as a secondary building unit (SBU), and link two Cd1 atoms of neighbouring SBUs by means of the coordination mode *b* (see Scheme 1) with a Cd···Cd distance of 17.36 Å. As a result, each entity is joined to other four establishing huge pseudo-rhombic rings of 17.4 x 28.8 $Å^2$ approximate dimensions. This grid can be regarded as a flat 2D Shubnikov **sql** layer with the $(4^4.6^2)$ point symbol from the topological point of view.[25]

Table 2. Selected bond lengths for compound **1**.[a]

Cd1–O1A	2.365(13)	Cd1–O2A(i)	2.281(17)
Cd1–O1A(i)	2.365(13)	Cd1–O1B	2.212(15)
Cd1–O2A	2.281(17)	Cd1–O1B(ii)	2.243(15)

[a] Symmetries: (i) –x – 1, –y, –z; (ii) –x – 1, y, z.

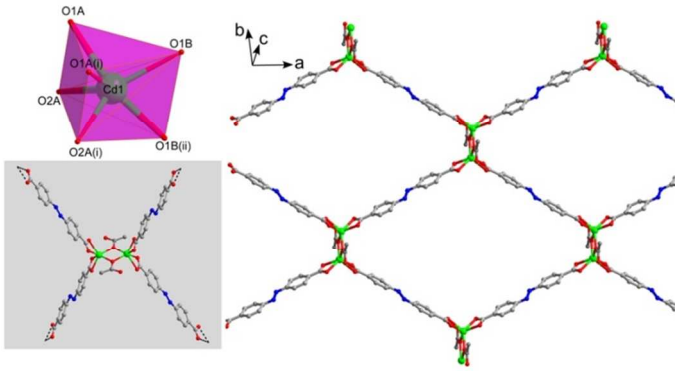

Figure 1. 2D layer of compound **1** showing the dinuclear entities with the atomic numbering scheme.

The piling of these layers in a parallel arrangement would give rise to a highly porous material with intermediate to huge channels depending on the lateral offset between the layers. However, the disorder present in the acetate anions, which prevents any clear hydrogen bonding receptor, makes the latter packing to be very unlikely and unstable. Instead, the 3D crystal building involves a two-fold interpenetration that significantly reduces the accessible volume (Figure 2).

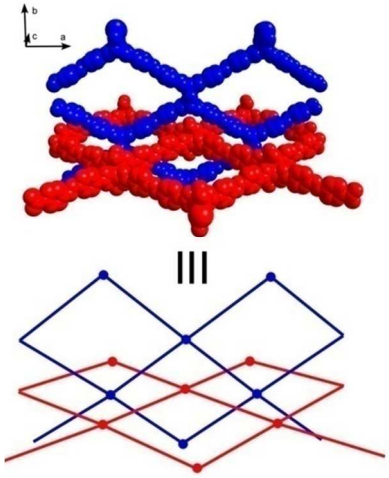

Figure 2. View of fragments of the perpendicular subnets entangled in compound 1. Schematic view is shown below: dinuclear entities (O) and ligands (–).

As a result, both subnets spread out almost perpendicular to each other (angle between mean planes of 89.47º). This entanglement problem is quite common in MOFs[26] since porous materials try to minimize the system energy through optimal filling of the void space, although the interpenetration may occur only if the pore space of an individual net is large enough as to accommodate an additional net as it is the case of bidentate long dicarboxylates. Hereafter, each of the subnets is subsequently piled up following an ABAB packing in such a way that these A and B parallel layers (identical subnet) cross the other subnet through the same pseudo-rhombic ring. Bridging acetate molecules get exposed perpendicularly to the layer and establish weak hydrogen bonding interactions (of the C–H···$O_{carboxylate}$ type) with the neighbouring interpenetrated layers (of the second subnet) (Figure 3). In spite of such an entanglement, the overall framework still contains narrow channels running along the crystallographic *c* axis that stand for the 32% of the unit cell volume, which are filled with dimethylammonium cations as well as highly disordered DMF molecules that could not be placed (Figure 4).

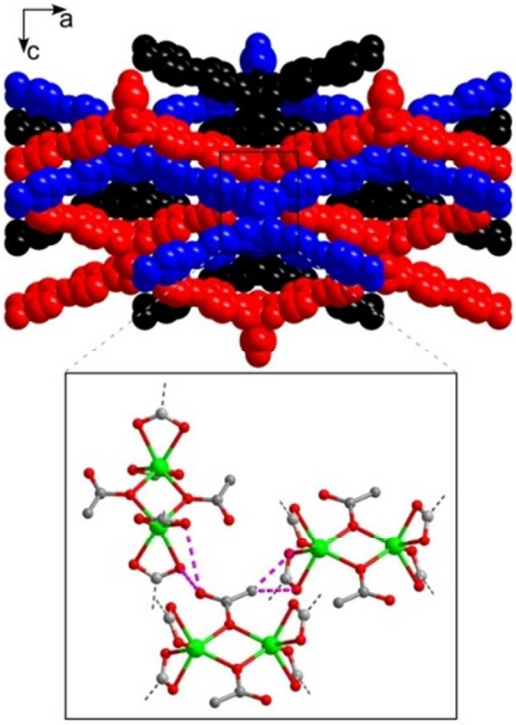

Figure 3. ABAB packing of layers of the same type of subnet (red and black) interpenetrated with a layer of the second subnet (blue). Caption shows hydrogen bonding interactions involving bridging acetate molecules and carboxylate oxygen atoms.

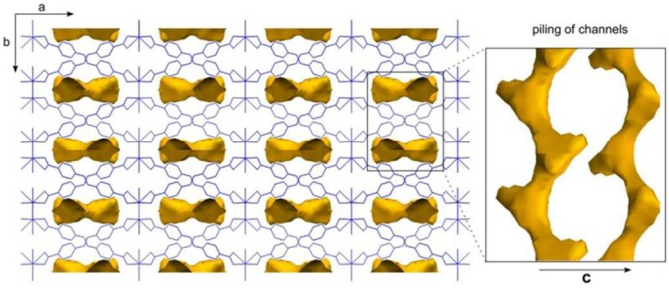

Figure 4. Crystal packing of compound **1** along crystallographic *c* axis showing the channels.

Crystal structure of compound **2** is also built up by the junction of dinuclear entities to lead to entangled 2D sheets. The main difference with regard to compound **1** is the bridging molecule that forms the centrosymmetric building unit, which is a carboxylic μ-O of the azdc ligand instead of the counterion afforded by the metal salt. Cd1 atom is linked to five carboxylate oxygen atoms from three azdc ligands that occupy the equatorial plane, whereas two oxygen atoms of crystallographically independent DMSO molecules complete the distorted pentagonal bipyramid environment (S_{PBPY} = 3.35) (Figure 5, Table 3).

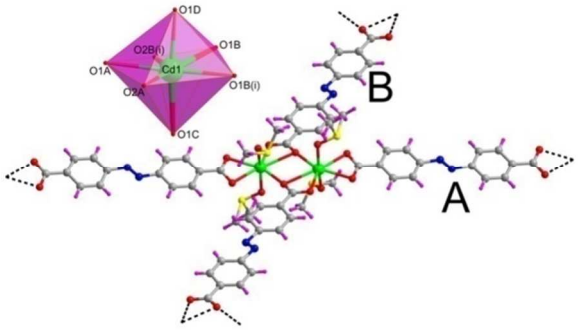

Figure 5. Excerpt of a layer of compound **2** showing the dinuclear building unit.

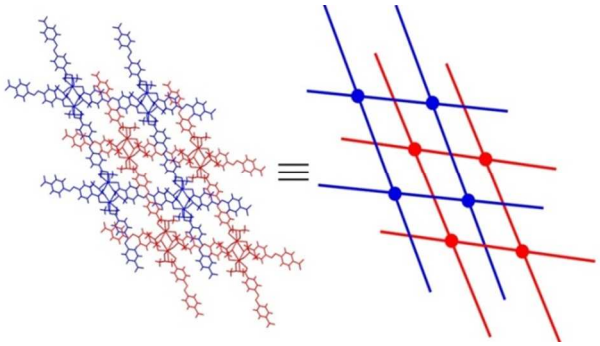

Figure 6. Interpenetration of the subnets of compound **2**.

Table 3. Selected bond lengths for compound **2**.[a]

Cd1–O1A	2.403(7)	Cd1–O2B(i)	2.294(7)
Cd1–O2A	2.396(6)	Cd1–O1C	2.288(8)
Cd1–O1B	2.327(7)	Cd1–O1D	2.292(7)
Cd1–O1B(i)	2.647(7)		

[a] Symmetries: (i) –x + 3/2, -y + 1/2, –z + 2.

Azdc ligands exhibit an almost planar conformation and two sort of bridging modes. On the one hand, μ_4-azdc ligands (B ligand) show coordination mode *c* (Scheme 1), to form the dinuclear entities through the μ-O1B bridge while one of the Cd(II) atoms takes part in a three-member chelating ring with the carboxylate group, which involves a lengthening of the Cd···Cd distance (4.05 *vs* 3.56 Å for compounds **2** and **1**). This building unit resembles that found for the related manganese(II) counterpart,[27] although in the latter the azdc ligand does not form a chelating ring. The resulting $[Cd_2(\mu_4\text{-azdc})]^{2+}$ chains running along the [110] direction are linked to each other by means of the carboxylate moieties of the μ-azdc ligands (A ligand, coordination mode *b*), which bite the cadmium atoms of two adjacent chains leaving an angle of ca. 66º between the μ-azdc connector and the cationic chain. Given the different coordination modes of azdc ligands, the second bridge imposes a shorter distance among the centroids of the dinuclear entities (16.4 *vs* 21.4 Å). This arrangement creates a similar rhomboid grid to that of **1**, belonging to the same topological class, in which the DMSO molecules arise perpendicularly from the flat layer. Owing to the occurrence of open rings within the layers and the lack of strong supramolecular interactions among them (except for weak C–H···O hydrogen bonds), they get doubly interpenetrated in such a way that one of the subnets blocks the free space of the rhombic rings of the other subnet by placing the dimeric entity at the centre of the ring. This fact does not allow a rhombic ring to be crossed by more than one subnet and forces the two subnets to be mutually folded at an angle of 45.9º between mean planes of both layers (Figure 6). The resulting entangled layers are further packed in a parallel fashion to lead to a 3D crystal building that contains isolated voids (12.7% of the unit cell volume) occupied by DMSO molecules.

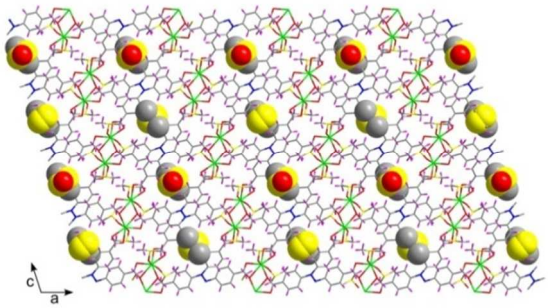

Figure 7. Packing of compound **2** showing crystallization DMSO molecules entrapped in the 3D framework.

Compound **3** crystallizes in the triclinic *P-1* space group and results from the pilling of 2D sheets generated by trinuclear SBUs. These SBU are centrosymmetric and contain two different cadmium(II) atoms (Figure 8). Cd1 lies on the centre of the unit and exhibits an almost ideal octahedral environment (S_{OC} = 0.20) established by six carboxylate oxygen atoms of six azdc ligands. Two Cd2 atoms occupy the edges of the unit and render a distorted capped octahedron (S_{COC} = 4.45) formed by six carboxylate oxygen atoms of three chelating independent azdc and the oxygen atom of the DMF molecule, which acts as a terminal ligand and prevents the SBU from further polymerization (Table 4). It must be noted that three Cd2–O_{carb} bonds, those establishing the chelating rings with the carboxylate groups, are remarkably longer than mean bond distances found for the previous compounds. Hence, all azdc ligands exhibit the same coordination mode (*c*, see Scheme 1) in such a way that three azdc bridge Cd1 with a Cd2 atom. Worthy to mention is that although acquiring the sharing the coordination mode, the Cd···Cd distance is remarkably shorter than in compound **2** (3.39 *vs* 4.05 Å) due to the non-planar disposition of the azdc linker with regard to the metallic core. As a consequence, six dicarboxylic linkers arise from the SBU in order to join it with six surrounding units, thus leading to a 2D network that exhibits triangular shaped rings and belongs to the Shubnikov **hxl** topological type and possesses the ($3^6.4^6.5^3$) point symbol (Figure 9). Within the sheets, metal atoms of the trimeric SBUs are spread out perpendicular to the mean plane whereas azdc ligands are arranged outwards it (forming an angle of nearly 45º with regard to the aromatic rings), which affords some corrugation to the sheet. The sheets are then piled up one another in a highly compact ABC fashion in which the DMF molecules of one layer pierce the rings of the upper and

lower sheets, which gives rise to an overall 3D packing with no solvent accessible voids.

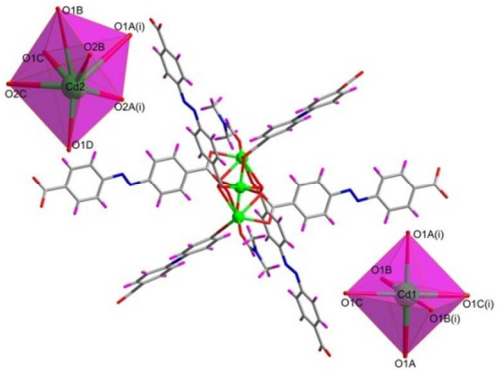

Figure 8. Trinuclear SBU of compound **3** showing the coordination environments of the two crystallographically independent Cd atoms.

Table 4. Selected bond lengths for compound **3**.[a]

Cd1–O1A	2.304(2)	Cd2–O1A(i)	2.503(2)
Cd1–O1A(i)	2.304(2)	Cd2–O1B	2.791(2)
Cd1–O1B	2.249(2)	Cd2–O1C	2.818(2)
Cd1–O1B(i)	2.249(2)	Cd2–O1D	2.222(2)
Cd1–O1C	2.272(2)	Cd2–O2A(i)	2.277(2)
Cd1–O1C(i)	2.272(2)	Cd2–O2B	2.201(2)
		Cd2–O2C	2.183(2)

[a] Symmetries: (i) –x + 3/2, -y + 1/2, –z + 2.

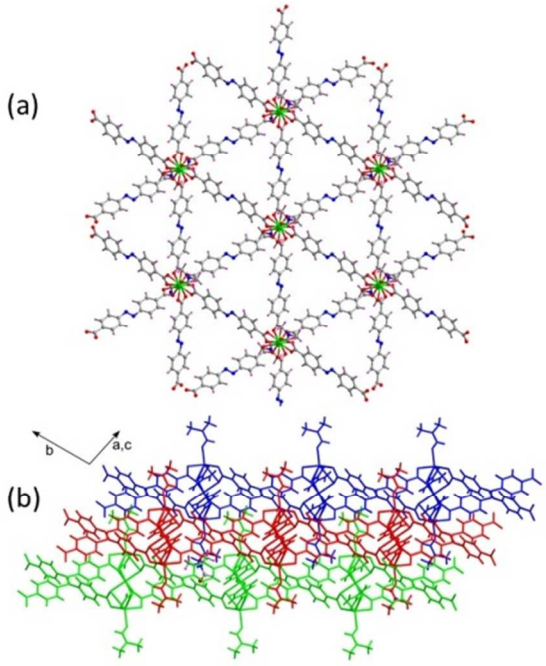

Figure 9. (a) Junction of the SBUs giving rise to the 2D sheet. (b) Pilling of the sheets along the [111] direction.

Compound **4** contains, in addition to azdc, pbptz coligands that act as pillaring linkers, which afford additional connectivity and give rise to a 3D framework. Given that azdc ligands show the coordination mode *a* (Scheme 1), their linkage to the zinc(II) atoms through two equivalent bidentate carboxylate groups (O3A and O4a atoms) forms dinuclear building units in which the metal atoms are placed out of the planes delimited by carboxylate moieties (Zn···Zn of 3.56 Å). The coordination environment of the crystallographically independent Zn1 atom (Figure 10, Table 5) is established by three carboxylate oxygen atoms and a nitrogen atom of the pbptz ligand, rendering a tetrahedron (S = 0.72).

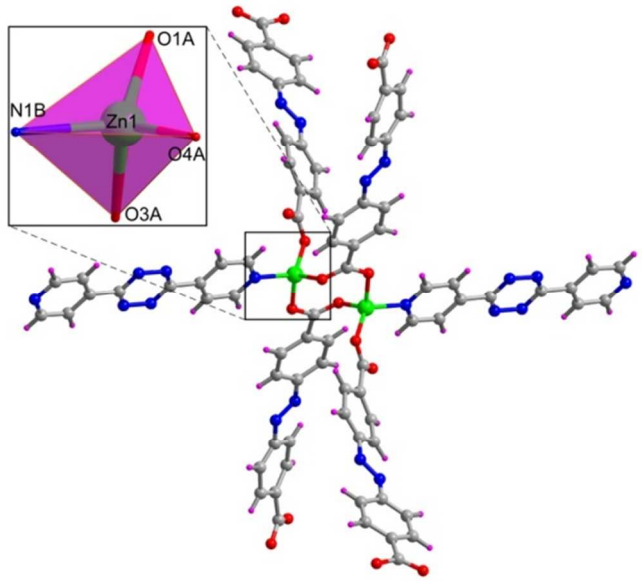

Figure 10. Excerpt of the crystal structure of **4** showing the dimeric SBU and coordination environment.

Table 5. Selected bond lengths for compound **4**.[a]

Zn1–O1A	1.918(6)	Zn1–O4A(ii)	1.951(4)
Zn1–O3A(i)	1.975(5)	Zn1–N1B	1.994(6)

[a] Symmetries: (i) –x + 3, y – 1/2, –z + 3/2; (ii) x – 1, –y + 1/2, z + 1/2.

Each building unit joins to four neighbouring ones by means of the coordination of the O1A atom of azdc ligands, whereas the O2A atom remains unbound at a large distance far beyond the bonding or semibonding limit estimated from the CSD database[28] (2.806 >> 2.479 Å). This asymmetric binding mode forces these linkers to be remarkably folded and twisted losing completely the characteristic planarity found in the preceding compounds (mean plane between the aromatic rings of 32.5º). As a consequence, the resulting 2D neutral $[Zn(\mu_3\text{-azdc})]_n$ layers show distorted square rings taking into account the centroids of the SBUs (Figure 11). The layers are then assembled together by the coordination pbptz ligands that arise from the building units almost perpendicular to the propagation of the layer, thus leading to a highly open 3D **pcu** network with the $(4^{12}.6^3)$ point symbol.

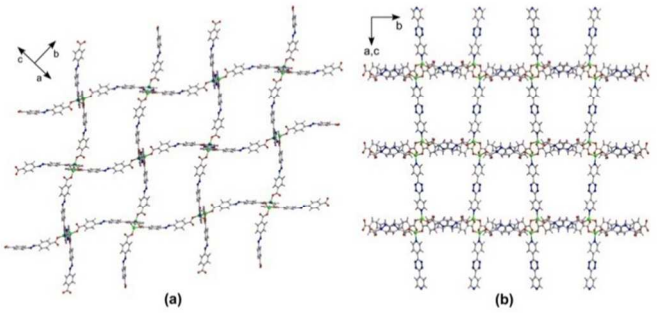

Figure 11. (a) Layer of compound **4** along the [-201] direction. (b) Pilling of the layers through the coordination of the pbptz ligand.

Despite the extremely high potential porosity of the network, most of the void percentage enclosed within the 3D architecture is eventually occupied by the occurrence of a 4-fold interpenetration. Even so, the overall packing retains a large accessible volume that accounts for the 32.5% of the unit cell volume. This volume is distributed in the form of infinite 1D helical channels running along the crystallographic a direction, which contain disordered DMF molecules

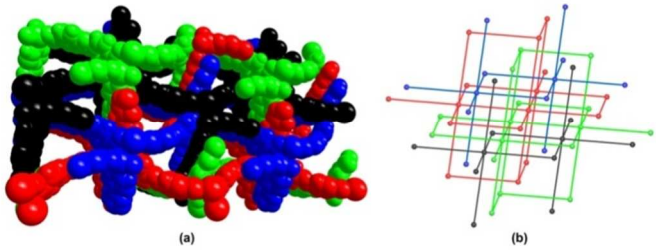

Figure 12. 4-fold interpenetration of entangled subnets in compound **4** viewed as (a) space-filling representation and (b) schematic view (dimeric entities as shown by closed balls).

The X-ray crystal structure analysis revealed that the basic building units of compound **5** are two crystallographically independent paddle-wheel entities (Figure 13) in which two zinc(II) atoms (Zn1 and Zn2 in the first unit, Zn3 in the second) are coordinated to the carboxylate oxygen atoms of four azdc ligands (coordination mode d), giving an intradimeric Zn···Zn distance of around 2.9 Å. The square pyramidal NO_4 donor sets (S_{SPY} of 0.31, 0.21, 0.27 for Zn1, Zn2, and Zn3) around the zinc centres (Table 6) are completed by the apical coordination of the pyrimidine nitrogen atoms of the pillaring μ-pbptz linkers. Despite the presence of two independent building units, the arrangement of the bridging azdc and pbptz ligands is so similar in both SBUs that they impose the same dimer···dimer distance when joining the SBUs together (16.95 and 17.88 Å, respectively). Therefore, given that the connectivity of the dimeric units is maintained, the resulting 3D backbone retains the **pcu** topology of compound **4**.

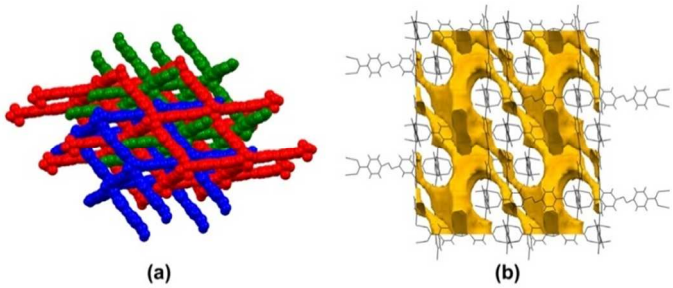

Figure 13. Coordination environment numbering, paddle-wheel entity and 3D backbone of compound **5**.

Table 6. Bond lengths of the coordination environments in compound **5**.[a]

Zn1–O1A	1.994(9)	Zn2–O2A	2.031(9)	Zn3–O1D	2.020(8)
Zn1–O1B	2.023(8)	Zn2–O4A	2.020(8)	Zn3–O2D(i)	2.049(9)
Zn1–O3A	2.037(8)	Zn2–O2B	2.027(8)	Zn3–O1E	2.020(9)
Zn1–O3B	2.004(9)	Zn2–O4B	2.032(9)	Zn3–O2E(i)	2.007(9)
Zn1–N1C	2.050(10)	Zn2–N16C	2.039(10)	Zn3–N1F(i)	2.029(10)

[a] Symmetry: (i) –x + 1, –y, –z.

Nevertheless, the 3D backbone of **5** can be referred to as a much more regular network than that of **4** owing to the more regular shape of the paddle-wheel entity, which entails a lesser torsion in the azdc ligands (from 0 to 20.1º for different ligands *vs* 32.5º). This fact permits the individual networks to be entangled into a triply interpenetrated framework, which reduces the size of the pores although they still stand for the 46.9% of the unit cell volume. This microporous backbone resembles that previously reported in which *trans*-bis-(4-pyridyl)ethylene replace pbptz ligands.[29] The 2D void system consists of wide and narrow channels cross-linked on the (101) plane, where DMF and water molecules are placed.

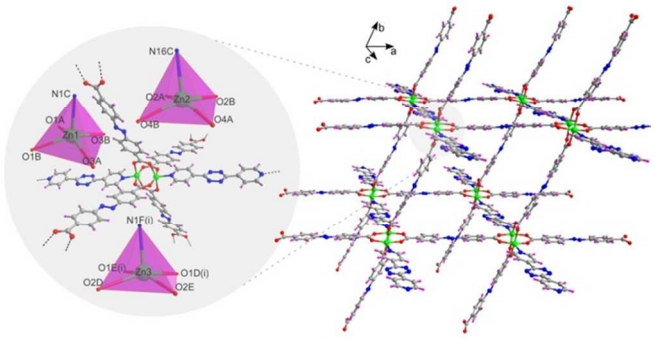

Figure 14. View of the 3D packing of compound **5** showing: (a) interpenetration between the three independent subnets and (b) 2D channel system.

3.3. Analysis of the porosity.

As previously observed, compounds **1**, **2**, **4**, and **5** show open 2D or 3D architectures containing large voids that are partially or fully occupied by additional networks due to the interpenetration phenomenon. This fact, although drastically

reduces the accessible surface area of the resulting framework, gives the opportunity to impose certain control on the size of the pores to access to void systems with narrower sections in which the adsorption of small molecules may be increased as a consequence of more effective framework···adsorbate interactions.[30] In order to get deeper insight the porosity features of these compounds, we have analyzed their pore-size distribution through a Monte Carlo procedure implemented in a code developed by Herdes and Sarkisov.[31] This method explores the free volume of the framework with a probe of incremental size that allows the examination of all pores contributing to the accessible volume, while it also provides useful information, such as specific surface area, which has proven to correlate well with the experimental data (Table 7).[32] In addition to the neat interpenetrated structures, non-interpenetrated networks have been studied as well with the aim of estimating the largest porosity available for each of the networks. In the light of the results, some interesting conclusions can be withdrawn. At first glance, 3D architectures (**4** and **5**) contain larger pores that lead to higher specific surface areas than those based on 2D layers (**1** and **2**) that are, in turn, rather non-porous. On the other hand, the comparison between interpenetrated and ideally non-interpenetrated structures show no clear correlation of the interpenetration degree with the pore size, since the latter is also dependent on the framework topology and geometry. However, when one pays attention to the maximum pore diameter, it can be observed that the value of the non-interpenetrated structure roughly doubles that of the interpenetrated one in all cases. This fact seems to indicate that the interpenetration degree acquired by a particular crystal structure will correspond to that better fits the latter relationship of the pore diameter.

Table 7. Geometrical analysis of the pore systems of compounds.

Comp.[a]	Geom. vol.[b]	He acc. vol.[c]	Surf. area[d]	Pore diameter[e]	
				Lim.	Max.
1	0.227	0.023	0	1.86	4.14
1-NoInt	0.986	0.973	2518.66	7.77	9.02
2	0.234	0.079	106.84	1.75	4.96
2-NoInt	0.901	0.750	2260.44	7.53	8.88
4	0.401	0.298	395.95	4.44	5.02
4-NoInt	1.822	1.580	4670.16	9.13	10.03
5	0.560	0.515	1043.89	5.09	7.31
5-NoInt	2.555	2.608	5317.79	11.63	13.91

[a] Analyzed compounds, considering the interpenetrated (bare number) and non-interpenetrated (number-NoInt) frameworks. [b] Geometric volume ($cm^3\ g^{-1}$). [c] Accessible volume for He ($cm^3\ g^{-1}$). [d] Accessible specific surface area ($m^2\ g^{-1}$). [e] Limiting and maximum pore diameters (Å).

3.4. Photoluminescence Properties.

Metal-organic frameworks based on d^{10} metal centres and organic ligands containing aromatic systems are promising candidates for developing new hybrid photoactive materials with potential application as light emitting diodes (LEDs) or chemical sensing.[33] Therefore, room temperature solid state emission spectra of the as-synthesized compounds **1**–**5** have been recorded. As previously reported, H_2azdc and pbptz ligands exhibit broad emission bands with the maxima peaking at 418 and 428/460 nm, respectively.[34] When excited at 310 nm, the main emissions of compounds **1** and **2** are slightly red shifted compared to the azdc ligand, whereas compound **3** shows two maxima at 418 and 436 nm (Figure 15). On the other hand, compounds **4** and **5** display intense emissions centred at 419 and 420 nm, thus attributed to azdc ligands. It can be presumed that all these emissions originate from $\pi^* \rightarrow n$ or even $\pi^* \rightarrow \pi$ transitions in which the energy gap slightly decreases (red shift or bathochromic emission) according to the coordination of the ligands to metal centres. The remaining weaker fluorescence peaks appearing at 485–490 nm, particularly for compounds **1**, **2**, and **4**; may be ascribed to ligand centred transitions whose intensity is considerably enhanced in comparison with the free ligand due to the increased rigidity of the ligands when bound to the metal centre, which effectively reduces the energy loss.

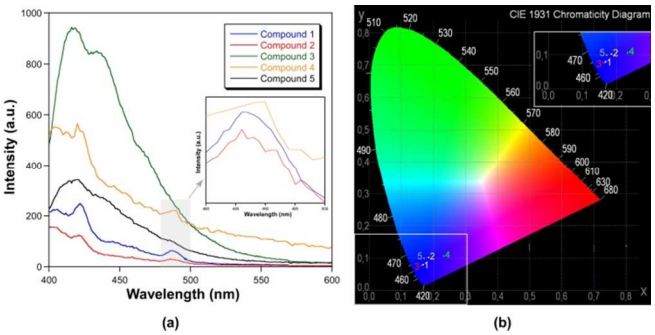

Figure 15. (a) Emission spectra of compounds **1**–**5**. Inset graphic corresponds to the magnified region of 480–500 nm. (b) Representation of the colour emissions of all compounds on the CIE 1931 chromaticity diagram.

The colour emissions have been located on the CIE 1931 chromaticity diagram (Figure 15b),[35] which shows that all compounds display blue fluorescence.

Conclusions

Five new compounds based d^{10} metal atoms and azobenzene-4,4'-dicarboxylic acid and 3,6-bis(4-pyridyl)-1,2,4,5,-tetrazine ligands have been obtained by solvothermal conditions. Crystal structures may be classified in terms of the dimensionality in two systems, for the coordination of the azdc ligand generates three types of 2D networks whereas the presence of a second ligand with the ability to act as a pillar gives rise to 3D frameworks. The structural diversity found in each system can be attributed to the employment of different solvents, counterions or metal-to-ligand stoichiometry, which modulates the coordination mode of the azdc ligand. Most of compounds feature open architectures that allow the growth of interpenetrated sub-nets given the length of the employed connectors. The interpenetration degree depends on the topology shown by the pristine network, ranging from 2-, 3- or even 4-fold entanglements, which allows controlling to an extent the size of the pores enclosed within the metal-organic

framework. The resulting void systems are characterized for possessing intricate narrow and broader sections that make the porous compounds of special interest for small molecules adsorption. On the other hand, fluorescence spectra reveal that these compounds show a blue emission probably due to transitions involving the π-conjugated systems of the ligands. Moreover, it has been observed how subtle structural modifications on the compounds lead to significant shifts in the CIE 1931 chromaticity diagram. All in all, coupling of the luminescence response and potential porosity of the compounds could signify their utility as photofluorescent sensors for small adsorbates.

Acknowledgements

This work was supported by the MEC of Spain (Project CTQ2011-24478) and the Junta de Andalucía (FQM-1484). Javier Cepeda acknowledges Universidad del País Vasco/Euskal Herriko Unibertsitatea for his postdoctoral fellowship and Jesus M. Ugalde for his guidance and support along the postdoctoral period.

Notes and references

a Departamento de Química Inorgánica, Universidad de Granada, 18071, Granada, Spain. Tel: 0034958240442; E-mail: antonio5@ugr.es
b Departamento de Química Aplicada, and c Departamento de Ciencia y Tecnología de Polímeros, Facultad de Químicas de San Sebastián, Universidad del País Vasco/EuskalHerrikoUnibertsitatea, Paseo Manuel de Lardizabal 3, 20018, San Sebastián, Spain. email: javier.cepeda@ehu.es.

1.- (a) H.-C. J. Zhou and S. Kitagawa, *Chem. Soc. Rev.*, 2014, **43**, 5415. (b) D. J. Tranchemontagne, J. L. Mendoza-Cortés and M. O'Keeffe, *Chem. Soc. Rev*., 2009, **38**, 1257. (c) V. Guillerm, D. Kim, J. F. Eubank, R. Luebke, X. Liu, K. Adil, M. S. Lah and M. Eddaoudi, *Chem. Soc. Rev*., 2014, **43**, 6141. (d) D. Bradshaw, S. El-Hankari and L. Lupica-Spagnolo, *Chem. Soc. Rev*., 2014, **43**, 5431. (e) J. W. Yoon, S. H. Jhung, Y. K. Hwang, S. M. Humphrey, P. T. Wood and J.-S. Chang, *Adv. Mater.*, 2007, **19**, 1830.

2.- (a) H.-C. Zhou, J. R. Long and O. M. Yaghi, *Chem. Soc. Rev*., 2012, **112**, 673. (b) R. Q. Snurr, J. T. Hupp and S. T. Nguyen, *AlChEJ*, 2004, **50**, 1090. (c) S. Pérez-Yáñez, G. Beobide, O. Castillo, M. Fischer, F. Hoffman, M. Fröba, J. Cepeda and A. Luque, *Eur. J. Inorg. Chem*., 2012, 5921. (d) O. K. Farha, I. Eyazici, N. C. Jeong, B. G. Hauser, C. E. Wilmer, A. A. Sarjeant, R. Q. Snurr, S. T. Nguyen, A. Ö. Yazaydin and J. T. Hupp, *J. Am. Chem. Soc*., 2012, **134**, 15016. (e) J.-R. Li, R. J. Kuppler and H.-C. Zhou, *Chem. Soc. Rev*., 2009, **38**, 1477.

3.- (a) L. J. Murray, M. Dinca and J. R. Long, *Chem. Soc. Rev*., 2009, **38**, 1294. (b) J. Cepeda, S. Pérez-Yáñez, G. Beobide, O. Castillo, J. A. García and A. Luque, *Eur. J. Inorg. Chem*., 2015, 2650. (c) S. Yang, X. Lin, A. J. Blake, G. S. Walker, P. Hubberstey, N. R. Champness and M. Schröder, *Nat. Chem*., 2009, **1**, 487.

4.- (a) J. Liu, L. Chen, H. Cui, J. Zhang, L. Zhang and C.-Y. Su, *Chem. Soc. Rev*., 2014, **43**, 6011. (b) J. Lee, O. K. Farha, J. Roberts, K. A. Scheidt, S. T. Nguyen and J. T. Hupp, *Chem. Soc. Rev*., 2009, **38**, 1450.

5.- (a) P. Horcajada, T. Chalati, C. Serre, B. Gillet, C. Sebrie, T. Baati, J. F. Eubank, D. Heurtaux, P. Clayette, C. Kreuz, J.-S. Chang, Y. K. Hwang, V. Marsadu, P.-N. Bories, L. Cynober, S. Gil, G. Férey, P. Couvreur and R. Gref, *Nat. Mater*., 2010, **9**, 172. (b) W. J. Rieter, K. M. Pott, K. M. Taylor and W. Lin, *J. Am. Chem. Soc*., 2008, **130**, 11584.

6.- (a) S. M. Cohen, *Chem. Sci*., 2010, **1**, 32. (b) A. Huang, H. Bux, F. Steinbach and J. Caro, *Angew. Chem. Int. Ed*., 2010, **49**, 4958.

7.- (a) H. Furukawa, N. Ko, Y. B. Go, N. Aratani, S. B. Choi, E. Choi, A. Ö. Yazaydin, R. Q. Snurr, M. O'Keeffe, J. Kim and O. M. Yaghi, *Science*, 2010, **329**, 424. (b) O. K. Farha, A. Ö. Yazaydin, I. Eryazici, C. D. Malliakas, B. G. Hauser, M. G. Kanatzidis, S. T. Nguyen, R. Q. Snurr and J. T. Hupp, *Nat. Chem*., 2010, **2**, 944. (c) H.-L. Jiang, T. A. Makal and H.-C. Zhou, *Coord. Chem. Rev*., 2013, **257**, 2232.

8.- (a) T. M. Reineke, M. Eddaoudi, D. Moler, M. O'Keeffe and O. M. Yaghi, *J. Am. Chem. Soc*., 2000, **122**, 4843. (b) B. Chen, M. Eddaoudi, S. T. Hyde, M. O'Keeffe and O. M. Yaghi, *Science*, 2001, **291**, 1021.

9.- O. M. Yaghi, *Nat. Mater*., 2007, **6**, 92.

10.- (a) S. Ma, D. Sun, M. Ambrogio, J. A. Fillinger, S. Parkin and H.-C. Zhou, *J. Am. Chem. Soc*., 2007, **129**, 1858. (b) O. Sekahah, H. Wang, M. Paradinas, C. Ocal, B. Schupbah, A. Terfort, D. Zacher, R. A. Fischer and C. Woll, *Nat. Mater*., 2009, **8**, 841.

11.- (a) O. K. Farha, C. D. Malliakas, M. G. Kanatzidis and J. T. Hupp, *J. Am. Chem. Soc.*, 2010, **132**, 950. (b) M. Dinca, A. Dailly, C. Tsay and J. R. Long, *Inorg. Chem*., 2008, **47**, 11.

12.- J. Zhang, L. Wotjas, R. W. Larsen, M. Eddaoudi and M. J. Zaworotko, *J. Am. Chem. Soc*., 2009, **131**, 17040.

13.- (a) P. Ryan, L. J. Broadbelt and R. Q. Snurr, *Chem. Commun*., 2008, 4132. (b) H. Frost and R. Q. Snurr, *J. Phys. Chem. C*, 2007, **111**, 18794. (c) D. H. Hung, D. Kim, T. B. Lee, S. B. Choi, H. Yoon, J. Kim, K. Choi and S.-H. Choi, *J. Phys. Chem. B*, 2006, **110**, 22987.

14.- S. Ma, J. Eckert, P. M. Forster, J. W. Yoon, Y. K. Hwang, J.-S. Chang, C. D. Collier, J. B. Parise and H.-C. Zhou, *J. Am. Chem. Soc.*, 2008, **130**, 15896.

15.- (a) P. K. Yadav, N. Kumari, P. Pachfule, R. Banerjee and L. Mishra, *Cryst. Growth Des*., 2012, **12**, 5311. (b) J. Yang, J.-F. Ma, S. R. Batten, S. W. Ng and Y.-Y. Liu, *CrystEngComm*, 2011, **13**, 5296. (c) Z.-F. Chen, Z.-L. Zhang, Y.-H. Tan, Y.-Z. Tang, H.-K. Fun, Z.-Y. Zhou, B. F. Abrahams and H. Liang, *CrystEngComm*, 2008, **10**, 217. (d) Y.-L. Liu, K.-F. Yue, B.-H. Shan, C.-J. Wang and Y.-Y. Wang, *Inorg. Chem. Commun*., 2012, **17**, 30.

16.- Z. H. Hu, B. J. Deibert and J. Li, *Chem. Soc. Rev*., 2014, **43**, 5815.

17.- Bruker Apex2, Bruker AXS Inc., Madison, Wisconsin, USA, 2004

18.- G.M. Sheldrick, SADABS, Program for Empirical Adsorption Correction, Institute for Inorganic Chemistry, University of Gottingen, Germany, 1996.

19.- A. Altomare, M. C. Burla, M. Camilla, G. L. Cascarano, C. Giacovazzo, A. Guagliardi, A. G. G. Moliterni, G. Polidori and R. Spagna, *J. Appl. Crystallogr*., 1999, **32**, 115.

20.- (a) G. M. Sheldrick, SHELX-2014, Program for Crystal Structure Refinement, University of Göttingen, Göttingen, Germany, 2014. (b) L. J. Farrugia, *J. Appl. Cryst*., 1999, **32**, 837.

21.- A. L. Spek, *J. Appl. Crystallogr*., 2003, **36**, 7.

22.- a) J. Juillard, *Pure Appl. Chem*., 1977, **49**, 885. b) T. Cottineau, M. Richard-Plouet, J.-Y. Mevellec and L. Brohan, *J. Phys. Chem. C*, 2011, **115**, 12269. c) K. O. Kongshaug, H. Fjellvag, B. Klewe and K. P. Lillerud, *MicroporousMesoporous Mater*., 2000, **39**, 333.

23.- a) H. Chun, D. N. Dybtsev, H. Kim and K. Kim, *Chem.–Eur. J*., 2005, **11**, 3521. b) H. J. Park and M. P. Suh, *Chem. Commun*., 2010, **46**, 610.

24.- (a) Z.-F. Chen, Z.-L. Zhang, Y.-H. Tan, Y.-Z. Tang, H.-K. Fun, Z.-Y. Zhou, B. F. Abrahams and H. Liang, *CrystEngComm*, 2008, **10**, 217. (b) S. Bhattacharya, U. Sanyal and S. Natarajan, *Cryst. Growth Des*., 2011, **11**, 735. (c) J. Cepeda and S. Pérez-Yáñez, *Eur. J. Inorg. Chem.*, 2014, 3221. (d) A. J. Calahorro, E. San Sebastian, A. Salinas-Castillo, J. M. Seco, C. Mendicute-Fierro, B. Fernández and A. Rodríguez-Diéguez, *CrystEngComm*, 2015, **17**, 3659.

25.- a) TOPOS: http://www.topos.ssu.samara.ru; b) V. A. Blatov, M. O'Keeffe and D. M. Proserpio, *CrystEngComm*, 2010, **12**, 44. c) V. A. Blatov, A. P. Shevchenko and D. M. Proserpio, *Cryst. Growth Des*., 2014, **14**, 3576.

26.- a) O. Shekhah, H. Wang, M. Paradinas, M. Ocal, B. Schüpbach, A. Terfort, D. Zacher, R. A. Fischer and C. Wöll, *Nat. Mater.*, 2009, **8**, 481. b) S. S. Han, D.-H. Jung and J. Heo, *J. Phys. Chem. C*, 2013, **117**, 71. c) T. K. Prasad and M. P. Suh, *Chem.–Eur. J.*, 2012, **18**, 8673.

27.- Y.-F. Han, Z.-B. Zheng, R.-T. Wu, Y.-F. Sun, X.-Y. Li and J.-K. Li, *Chin. J. Inorg. Chem*., 2010, **26**, 1125.

28.- F. H. Allen, *Acta Crystallogr., Sect. B*, 2002, **58**, 380.

29.- B. Chen, S. Ma, E. J. Hurtado, E. B. Lobkovsky and H.-C. Zhou, *Inorg. Chem*., 2007, **46**, 8490.

30.- a) A. Torrisi, C. Mellot-Draznieks and R. G. Bell, *J. Chem. Phys.*, 2009, **130**, 194703. b) L. Valenzano, B. Civalleri, S. Chavan, S. Bordiga, M. H. Nilsen, S. Jakobsen, K. P. Lillrud and C. Lamberti, *Chem. Mater.*, 2011, **23**, 1700. c) J. Cepeda, S. Pérez-Yáñez, G. Beobide, O. Castillo, M. Fischer, A. Luque and P. A. Wright, *Chem.–Eur. J.*, 2014, **20**, 1554.

31.- C. Herdes and L. Sarkisov, *Langmuir*, 2009, **25**, 5352.

32.- T. Duren, F. Millange, G. Férey, K. S. Walton and R. Q. Snurr, *J. Phys. Chem. C*, 2007, **111**, 15350.

33.- a) Y. Cui, Y. Yue, G. Qian and B. Chen, *Chem. Rev*., 2012, **112**, 1126. b) Z. Hu, B. J. Deibert and J. Li, *Chem. Soc. Rev*., 2014, **43**, 5815.

34.- a) J.-S. Guo, G. Xu, G.-C. Guo and J.-S. Huang, *Cryst. Gowth Des*., 2013, **13**, 2642. b) J. Li, Y. Peng, H. Liang, Y. Yu, B. Xin, G. Li, Z. Shi and S. Feng, *Eur. J. Inorg. Chem*., 2011, 2712.

35.- a) A. D. Broadbent, *Color Res. Appl .K*, 2004, **29**, 267. b) T. Smith and J. Guild, *Trans. Opt.*, 1931, **33**, 3.

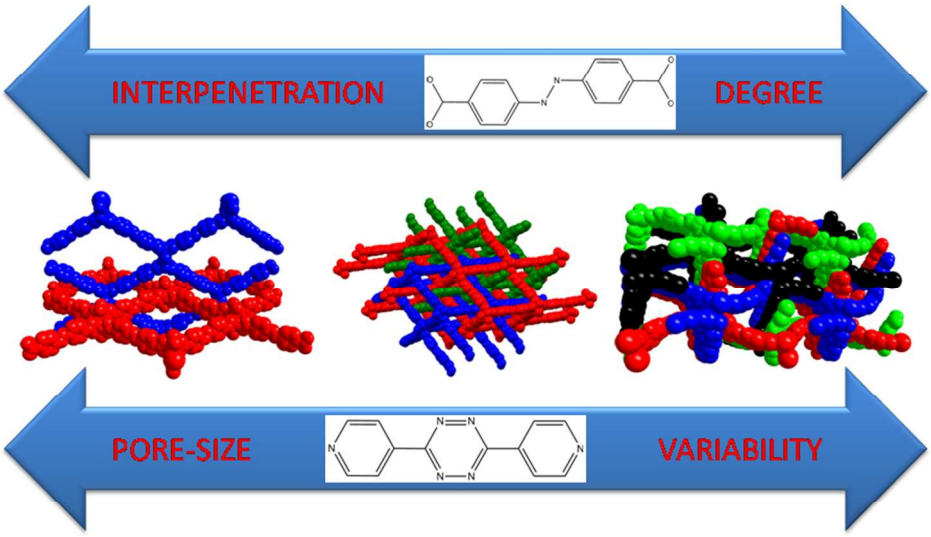

The pore size can be tuned in a series of Metal-Organic Frameworks based on azobenzene-4,4'-dicarboxylate and 3,6-bis(4-pyridyl)-1,2,4,5-tetrazine with Zn(II) or Cd(II) metal atoms by means of the interpenetration degree acquired by the structure. These structural features promote subtle shifts in the blue emission of the compounds.
254x190mm (96 x 96 DPI)